International Journal of Engineering

Journal Homepage: www.ije.ir

Effect of Graphite Addition on the Microstructure, Mechanical Properties and Oxidation Resistance of HfB_2-SiC Composites Prepared by the SPS Method

M. Sakvand[a], M. Shojaie-Bahaabad*[a], L. Nikzad[b]

[a] *Faculty of Chemical and Materials Engineering, Shahrood University of Technology, Shahrood, Iran*
[b] *Department of Ceramics, Materials and Energy Research Center, Karaj, Iran*

PAPER INFO

Paper history:
Received 09 March 2022
Received in revised form 06 May 2022
Accepted 20 May 2022

Keywords:
HfB_2-SiC Composite
Spark Plasma Sintering
Ultra-high Temperature Ceramic
Oxidation
Graphite

ABSTRACT

In this study, HfB_2-SiC-graphite composites were fabricated using spark plasma sintering at 1900 ℃ for 10 min. The effect of graphite content on the microstructure and mechanical properties was studied; also, oxidation resistance of the prepared composites was investigated at 1400 ℃ for 32 h. Weight changes and thickness of the formed oxide layer were measured. The relative density, toughness and strength of the SPSed composites increased with raising graphite up 2.5 wt% and then decraesed. On the other hand, the hardness of the composites was decreased when graphite was added. Oxidation resistance of the composites was, thus, improved following graphite addition up 2.5 wt%, while the ecessive quantity of graphite caused poor oxidation resistance of the composites.

doi: *10.5829/ije.2022.35.10a.06*

1. INTRODUCTION

Compounds such as borides, carbides and nitrides of the IV-V group intermediate metals, which have melting temperatures above 3000 °C [1], are known as ultra high temperature ceramics (UHTCs) [2]. Good oxidation resistance [3] and high thermal and electrical conductivity [4] of diboride refractory compounds, as compared to other intermetallic compounds (carbides, nitrides), have led to extensive research on diborides such as (Ta, Nb, Hf, Zr, Ti)B_2 [5]. Among intermediate metal diborides, HfB_2 and ZrB_2 are the most suitable options for high temperature applications such as turbine blade coatings, furnace elements, high temperature electrodes, rocket motors, sharp noses and heat resistant systems [6]. HfB_2, compared to other compounds at high temperature ceramics family, has received more attention by researchers due to its higher thermal conductivity and chemical stability [7]. However, like many refractory ceramics, strong covalent bonds and low self-diffusion coefficient in HfB_2, as well as the presence of oxide contaminants, can limit the complete densification of these ceramics. Numerous studies have been reported on the synthesis and sinterability of HfB_2 ceramics using mechanical alloying, borothermal or carbothermal solid state reduction, Self-propagating high-temperature synthesis (SHS), non-pressure sintering, reactive hot press, hot isostatic press and spark plasma sintering (SPS) [8-12]. In the recent years, several researchers have used the SPS method for the compaction of HfB_2 ceramics. This method simultaneously employs a direct pulse current and an external axial force on a compacted powder in graphite die to accelerate sintering. High heating rate (100 °C/min) and lower sintering temperature, compared to other methods, can lead to a finer microstructure. In addition, in this method, due to the spark between the powder particles and the use of direct pulse flow, materials with poor sinterability can be successfully compacted [13]. Also, up to now, metal additives (Fe, Ni, Co, W), nitrides (AlN, HfN, Si_3N_4), carbides (SiC, HfC, WC, VC) and desilicides ($MoSi_2$, $HfSi_2$, $TiSi_2$, $TaSi_2$) have been used to improve the sintering and mechanical properties of HfB_2 ceramics [14-22]. The addition of SiC as the most common carbide

*Corresponding Author Institutional Email: mshojaieb@shahroodut.ac.ir (M. Shojaie-Bahaabad)

Please cite this article as: M. Sakvand, M. Shojaie-Bahaabad, L. Nikzad, Effect of Graphite Addition on the Microstructure, Mechanical Properties and Oxidation Resistance of HfB_2-SiC Composites Prepared by the SPS Method, ***International Journal of Engineering, Transactions A: Basics***, Vol. 35 No. 10, (2022), 1867-1876

additive to HfB_2 not only improves its sinterability, but also enhances its mechanical properties and oxidation resistance. Oxidation of HfB_2 occurs at low temperatures (<1000 °C). Reports indicate that the presence of 10-30 vol% SiC is required to obtain the oxidation resistance of HfB_2 ceramics. The presence of SiC improves the oxidation resistance of these composites by forming a borosilicate glass layer and also protects the HfB_2 - SiC composites up to 2000 °C in an oxidized atmosphere without air flow. One model suggests that active oxidation of SiC below the borosilicate glass layer leads to the formation of a Si-depleted layer [23, 24]. As the SiO_2 glass layer acts as a protective barrier, the oxygen activity under the glass layer is much lower than that in its surface in the presence of air. Under the reducing conditions, SiO (g) and CO (g) have higher vapor pressures in comparison to SiC below the SiO_2 layer, which can lead to the active oxidation of SiC. It has been reported that the addition of graphite to the ZrB_2-SiC composite could affect the formation of the Si-depleted layer below the SiO_2 layer [25, 26]. In addition, the increase in the siterability, toughness and microstructure of ZrB_2-SiC composites has been observed due to the presence of carbon [27-30]. So far, the effects of different sintering methods, sintering temperatures and different values of SiC on HfB_2-SiC composites have been extensively investigated [8-13]. The present study , thus, focused on the fabrication and estimation of the mechanical and oxidation properties of HfB_2-SiC-C composites by the SPS method. The aim of the present study was, therefore, to study the effect of different amounts of graphite on the microstructure and mechanical and oxidation properties of the HfB_2-SiC composite.

2. MATERIALS AND METHOD

Commercial HfB2 (< 2 µm, purity 99%, Beijing Cerametek Materials Co., China) as the matrix, and SiC (< 10 µm, purity 99%, Xuzhou Co., China) and graphite flakes (< 50 nm, purity 99.9%, Qingdao Tiansheng Graphite Co.,China) as additives were used to synthesize HfB_2-20 vol%SiC-C. Figure 1 shows the morphological characteristics of the starting powders. As can be seen, the morphology of HfB_2 and SiC particles was spherical and angular, respectively. Some oxide impurities (HfO_2 and B_2O_3) might exist on the surface of HfB_2 particles. Also, graphite was morophologically nano-sized flakes. Graphite flakes were introduced at two content levels (2.5 and 5 wt%) to the HfB_2 powders. At first, HfB_2 and SiC powder mixtures were milled by high-energy planetary milling using balls and a WC-Co cup at 300 rpm for 3 h in ethanol medium, with the weight ratio of balls to powders being 10: 1. The graphite nano-flakes were ultrasonically stirred in diluted ethanol for 1 h; then, the mixtures of HfB_2 and SiC powder was added to the

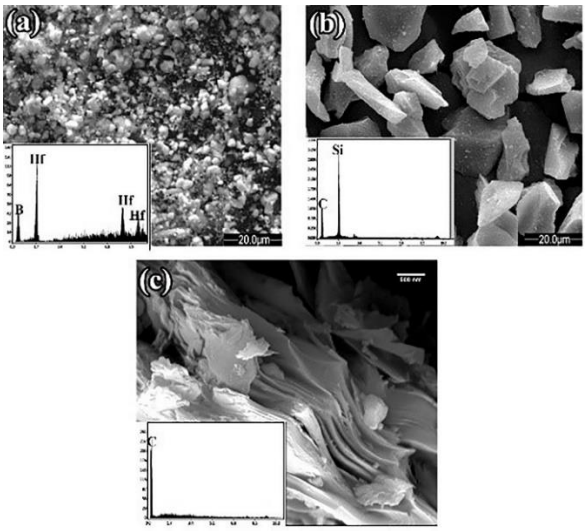

Figure 1. SEM image of starting powders (a) HfB_2, (b) SiC and (C) graphite

slurry. The slurry was dried at 60 °C for 2 h and then sieved using the mesh number 100. HfB_2-20SiC composites were fabricated by the SPS method at 1900 °C for 10 min in the vacuum of 0.05 mbar and under 40 MPa pressure. The obtained composites with different amounts of graphite, including 0, 2.5 and 5 wt%, were named as G0, G2.5 and G5, respectively. The microstructure of the composites was investigated without thermal or chemical etching. Relative density values and porosity percent of the composites were then calculated by the Archimedes method in distilled water. Theoretical density was calculated according to the law of mixtures. Phase analysis of the composites was then performed using X-ray diffraction pattern (XRD, Philips, Model: X'Pert MPD, Tube: Co, and l: 1.78897 Å); their surface and microstructure were examined using field emission scanning electron Microscope (FESEM, TESCAN, Model: MIRA) equipped with energy dispersive spectroscopy (EDS). The average grain size of the composites was measured using the MIP Cloud software. The hardness of the composites was measured using a Vickers hardness tester under 1 kg with a loading time of 10 s. The flexural strength of the composites was evaluated using a three-point flexural machine (Zwick Roell SP600, Germany) with a loading rate of 0.05 mm/min. Oxidation tests were performed in an electric furnace at 1400 °C for 32 h. The oxidation resistance of the composites was evaluated according to the weight changes and thickness of the oxide layer after oxidation.

3. RESULTS AND DISCUSSION

The displacement-temperature-time (DTT) curve of the composites is shown in Figure 2. In the displacement-time curve of the samples, three regions could be seen. In

the first region, the displacement was due to the rearrangement of the particles, the increase of the contact surface of the particles, the creation of more sparks, and the improved thermal efficiency due to the rise of pressure and temperature. With the improvment of thermal efficiency, the local temperature at the particle contact surface was increased rapidly, causing a change in the temperature-time curve. This phenomenon has also been reported by other researchers [31-33]. In the second region, there was a sharp change in the displacement curve. This sharp change was due to the increase in pressure on the powder particles up to a final pressure of 40 MPa. Bulk deformation occurred in this area due to high temperature, neck growth between particles, full contact of the particles and noticeable contraction. In samples G2.5 and G5, in the second region, the displacement was first decreased and then increased. The initial decrease indicated the expansion caused by the gases created by the evaporation of impurities and surface oxide contaminants due to the presence of the graphite additive. In the third region of the displacement-time curve, the increase in the slope of the curve was very slow, thus indicating that the sintering process of the composites was complete. In the third region, the displacement-timecurve was almost smooth, thus showing the complete compaction of these composites [32]. Oxide contaminants on the surface of the HfB_2 powder could increase the vapor phase transfer velocity and particles coagulation, and reduce the direct contact of the particles and the sintering driving force. It seems, therefore, that the contact surface of HfB_2 particles was increased through the reaction of oxygen impurities (HfO_2 and B_2O_3) with SiC [34].The result of this chemical reaction is gaseous products such as SiO, CO and BxOy;these, before the production of gaseous products, cause the formation of the liquid phase, finally increasing the sinterability of the HfB_2 powder [36]. Comparison of the displacement-time curve, as can be seen in Figure 2, showed that the sinterability was improved by adding 2.5 wt% graphite. This was due to the lubricating properties of the layered graphite and the increased particle slip as a result of improving the sinterability of the composites [27]. It seems, therefore, that with increasing the amount of the graphite additive up to 5 wt% in the composite, due to more reaction with surface oxide contaminants and removal of them, the amount of liquid phase was reduced; as a result, the rate of compaction and shrinkage was decreased. The density and apparent porosity of the composites are given in Table 1. By increasing the amount of graphite to 2.5 wt%, due to the effect of graphite on removing surface impurities on SiC and HfB_2 particles and helping to improve the densification of the composite, density was increased, while the percentage of porosity in the composite was decreased. As the amount of graphite was increased to 5 wt%, density was decreased, while porosity was raised. With increasing graphite up to 5 wt%, due to graphite agglomeration and the space between graphite layers, as a result of the lack of the proper compaction of graphite layers, there was a decrease in density and an increase in the porosity of the composites [35]. The XRD patterns of the composites after the SPS process are shown in Figure 3. As shown, HfB_2 and SiC phases were observed in the samples and there were no unwanted phases in the composites. Figure 4 shows the SEM images along with the elemental analysis (EDS) of the composites surface after the SPS process. SEM image (Figure 4a) showed the HfB_2-SiC composite (G0) surface areas with severe agglomeration. EDS analysis of the G0 sample surface also revealed that the existing agglomerates contained HfB_2 particles. The presence of this agglomerate could be due to the high density difference of HfB_2 (10.5-11.2 g/cm^3) and SiC (3.2 g/cm^3), and graphite (2.25 g/cm^3). According to the SEM images in the G2 and G5 samples, the phases forming the composite were uniformly distributed on the

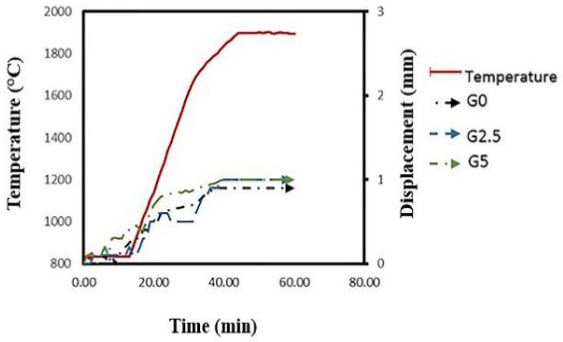

Figure 2. The displacement-temperature-time (DTT) curves of the sintered composites, (a) G0, (b) G2.5 and (c) G5

TABLE 1. Physical properties of the sintered composites

Sample	True density (gr/cm^3)	Apparent density (gr/cm^3)	Relative density (%)	Total porosity (%)	Open porosity (%)	Closed porosity (%)
G0	8.75	8.62	98.5	1.5	0.98	0.52
G2.5	8.07	8.02	99.39	0.6	0.28	0.32
G5	7.08	6.87	97.1	2.9	0.96	1.94

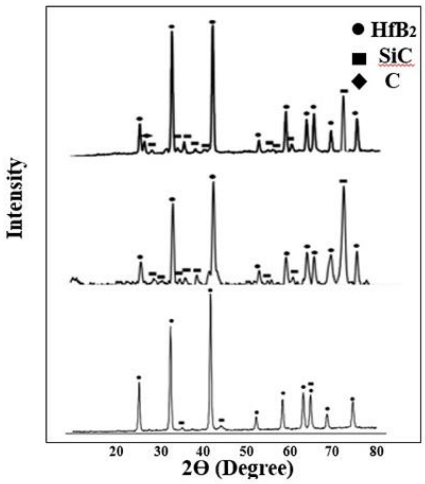

Figure 3. XRD patterns of (a) G0, (b) G2.5 and (c) G5

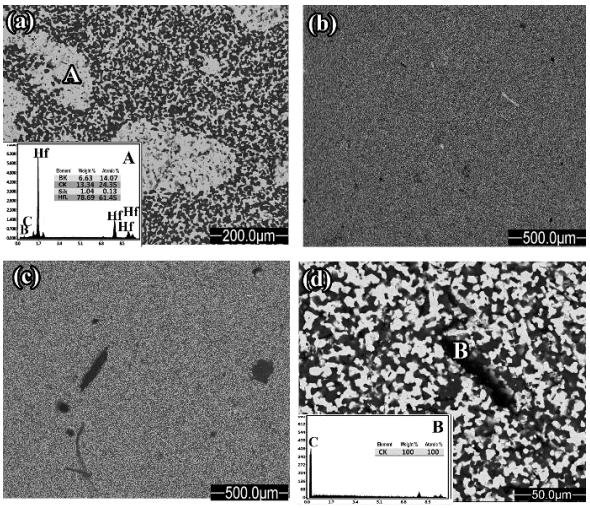

Figure 4. FESEM images and EDS analysis of the sintered composites: (a) G0, (b) G2.5 and (c,d) G5

surface; with increasing the amount of graphite up to 5 wt%, the formation of graphite agglomerates was observed. SEM images along with the EDS analysis of the HfB_2-SiC composites at higher magnifications are shown in Figure 5. As can be seen, the structure was homogeneous and the particles were evenly distributed. Two areas were clearly observed on the surface of the composites. According to the EDS analysis, the dark areas were related to the SiC phase and the light ones were associated to the HfB_2 phase. According to the SEM images, except for some cavities due to surface polishing after the sintering process, no traces of porosity were visible, thus confirming the results obtained for the density of the composites. In addition, microcracks were observed in HfB_2 (white arrow) particles. Differences in the thermal expansion coefficients of these two phases could lead to compressive or tensile residual stresses in

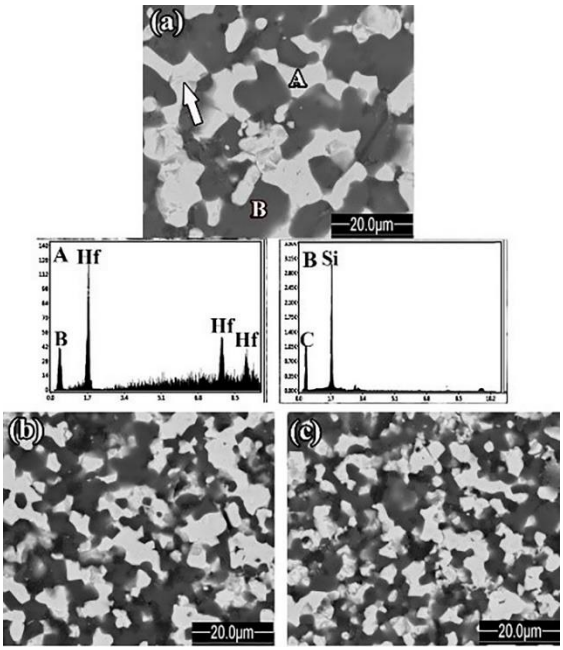

Figure 5. High magnification of FESEM images and EDS analysis of the sintered composites: (a) G0, (b) G2.5 and (c) G5

the deboride matrix, eventually creating micro-cracks [36, 37]. The mean grain size curve of HfB_2-SiC composites after the sintering process is shown in Figure 6. The grain size was reduced by adding graphite to the HfB_2-SiC composites. The grain size of prepared G0, G2.5 and G5 composites were 5.3, 3.3 and 2.4 µm, respectively. Researchers have shown that the presence of oxide impurities on the surfaces of boride particles causes HfB_2 grains to coagulate. It seems, therefore, that adding more graphite, by removing oxide impurities, could prevent the growth of HfB_2 grains, thus causing the structure to become fine. Figure 7 shows the scanning electron images of the fracture ross-section of the composites after the SPS process. According to the images, the composites had a good density and the formation of a neck between the particles, which accelerated the compaction process (thin arrow), was evident. Although neck formation is the characteristic of the controlled sintering process, it seems that applying pressures up to 40 MPa at high temperatures during the SPS process could deform the plastic at the HfB_2 grains.

The deformed HfB_2 grains in the form of a uniform polygonal surface could be distinguished from the other grains in Figure7 (thick arrow). Adding SiC particles to the HfB_2-based composites could cause the formation of an intergranular liquid phase during the SPS process. The presence of an oxide layer on the surface of non-oxide particles (such as HfO_2, SiO_2 and B_2O_3) caused the formation of borosilicate glass phases. . Sabree et al. [38] in their research work on the ZrB_2-SiC composite

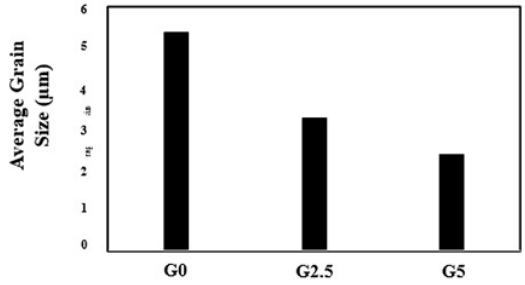

Figure 6. HfB_2 grain size of the sintered composites

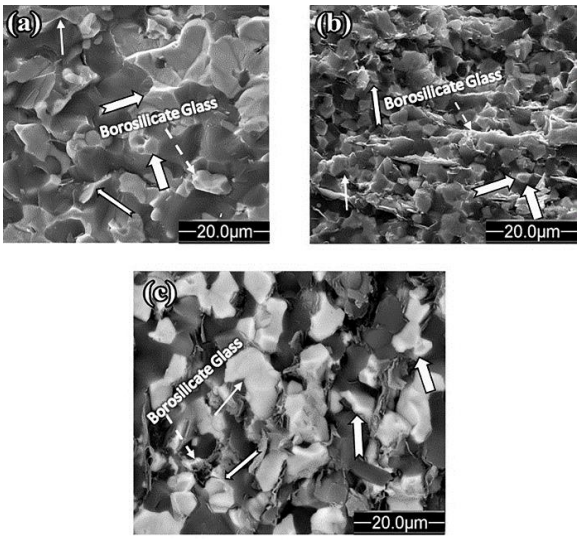

Figure 7. FESEM images of the fracture surface of the sintered composites, (a) G0, (b) G2.5 and (c) G5

sintered by the hot pressing method, also stated that the glass phase in SEM images was visible in the form of a coating, a uniform and brittle fracture surface or a low thickness layer. Such a glass phase was clearly visible in the SEM images of the cross-sections of the composites prepared in the present research work (dashed flash).

In the HfB_2-SiC composites cross-section images with different amounts of graphite, graphite layers were observed in the cross section. This indicated that graphite was not converted to new phases. Thus, it could be concluded that the sintering and compressibility in the HfB_2-SiC-C systems was non-reactive. According to the images, the graphite layers distributed between the grains showed that they were placed between the grains by applying pressure during the SPS process with a specific orientation. Shahedi et al. [35] also reported the orientation of graphite when applying pressure to the microstructure with a micron grain size. The fracture surface of the sintered composites showed a combination of intragranular and intergranular fractures. Particles pull out and sharp edges could be seen in the images, which could be related to the intergranular fracture that had occurred in grain boundaries (thin arrows) [39]. In some areas, especially when comparing surfaces with the abnormal grain growth to other grains, wide and smooth surfaces could be seen, thus indicating the intragranular fracture (thick arrows). The results of the mechanical analysis for the HfB_2-SiC composites after the SPS process are given in Table 2. According to the results obtained from the hardness test, with increasing the amount of graphite in the composites, hardness was decreased from 19.04 to 10.16 GPa and then to 6.11 GPa.

Although the composite containing 2.5 wt% had a high density, due to the inherent softness of graphite, hardness was decreased. With increasing the amount of graphite, hardness was further decreased in the G5 sample. Among the effective factors in the flexural strength of materials, grain size and density or porosity can be noted; so, the smaller the grain size and the higher the density, the higher the flexural strength of the composite. In the samples, flexural strength was enhanced with increasing graphite up to 2.5 wt% due to decreasing the matrix grain size and increasing the density,; meanwhile, with further increasing the graphite content to 5 wt%, flexural strength was decreased due to the decrease in the density of the composite. Figure 8 shows the effect of the Vickers hardness test on the HfB_2-SiC composites. As can be seen, in the G2/5 sample, due to the high density of this sample, as compared to others, the effect of hardness was regular and no deformation was observed around it. In other samples, the hardness effect was more irregular due to porosity.The HfB_2-SiC-C X-ray diffraction pattern after oxidation at 1400 °C for 32 h is shown in Figure 9. According to the XRD results, $HfSiO_4$ and HfO_2 phases were observed in these composites after oxidation at 1400 °C for 32 h. The main phase was $HfSiO_4$, although some HfO_2 phase was also formed during the oxidation test. The formation of the $HfSiO_4$ silicate phase due to the locking effect of this phase and finally, the non-defective and crack-free oxide coating on the composite surfaces could cause the resistance to the oxidation of HfB_2 base composites [42]. HfO_2 and $HfSiO_2$ formation and oxidation of graphite were formed according to the equation of the following reactions [40-42]:

$$2SiC(s) + 3O_2(g) = 2SiO_2(l) + 2CO(g) \quad (1)$$

$$2HfB_2(s) + 5O_2(g) = 2HfO_2(s) + 2B_2O_3(l) \quad (2)$$

$$SiO_2(l) + HfO_2(s) = HfSiO_4(s) \quad (3)$$

TABLE. 2. Mechanical properties of the sintered composites

Sample	Hardness (GPa)	Strength (MPa)
G0	8.75	8.62
G2.5	8.07	8.02
G5	7.08	6.87

$$2\,C\,(s) + O_2\,(g) = 2CO\,(g) \quad (4)$$

$$B_2O_3\,(l) = B_2O_3\,(g) \quad (5)$$

It has been reported in the literature that molten B_2O_3 evaporates at temperatures above 1100 °C; its evaporation rate is faster than the formation rate of the molten B_2O_3 at the 1100-1400 °C range, according to the reaction (5) [42]. Thus, B_2O_3 phase was not observed in the X-ray pattern of the composites after oxidation. The SEM image of the surface of the composites after oxidation at 1400 °C for 32 h is shown in Figure 10. As can be seen, the surfaces of the composites were coated with a glass layer of SiO_2.

Oxidation of SiC particles, at temperatures above 1100 °C resulted in the formation of a glass layer of SiO_2 on the surface of the composites. Except for the G0 specimen, the glass layer was evenly distributed on the HfB_2-SiC composite surface. Two types of bubbles were observed on the surface of this oxide layer. Some of these bubbles had grown to the surface (Figure 10a), but some had not been opened to the surface (Figure 10b). Researchers believe that due to the high viscosity of the glass layer, this layer could not flow near these bubbles and cover the open bubbles. These bubbles could be attributed to the accumulation of gaseous products due to the active oxidation of SiC at the high temperature of 1400 °C (reaction (6)), as well as the evaporation of B_2O_3 [43].

$$SiC\,(s) + O2(g) = SiO\,(g) + CO\,(g) \quad (6)$$

As reported in the previous sections, HfB_2 agglomerates were observed in the G0 sample of the composite. Thus, due to the inhomogeneous and random distribution of SiC particles in the composite, the glass layer was formed locally on the composite surfaces; as a result, it was expected that the oxidation resistance of this composite would be decreased [5]. The white crystals with different sizes and shapes were observed on the surface of the composites after oxidation. According to the XRD results, these crystals were HfO_2 and $HfSiO_4$. According to results related to the ZrB_2-SiC oxidation resistance by De-We, the formation of crystalline phases in the present study could be described as follows. After forming HfO_2 and SiO_2, according to reactions (1) and (2), HfO_2 was first dissolved in the SiO_2–B_2O_3 melt, forming SiO_2-B_2O_3 (HSB) liquid in the glass layer. Then, as the oxidation process progressed, the HSB liquid flowed on the top of the glass layer. When B_2O_3 was evaporated, HfO_2 particles were precipated from the

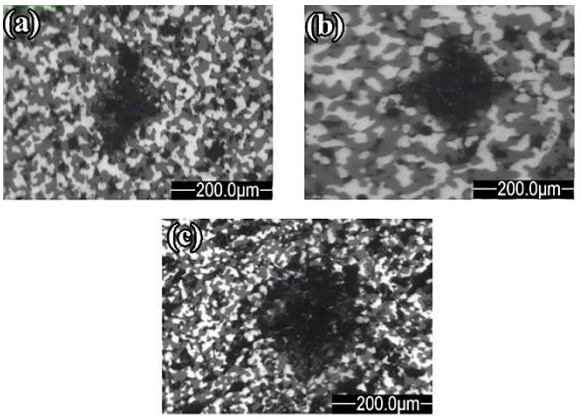

Figure 8. FESEM images of the Vickers indenter effect of the sintered composites: (a) G0, (b) G2.5 and (c) G5

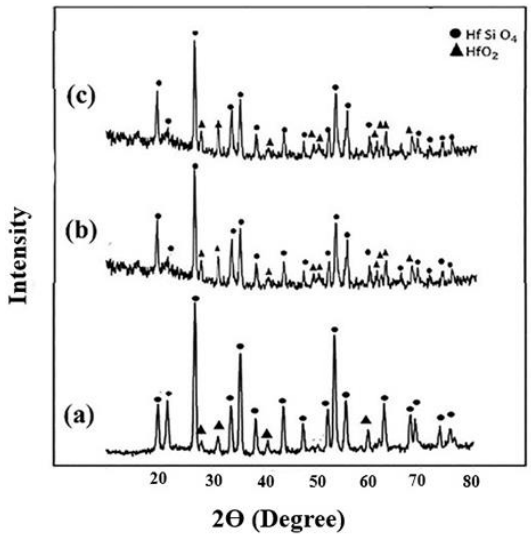

Figure 9. XRD patterns of the samples after the oxidation test at 1400 °C for 32 h: (a) G0, (b) G2.5 and (c) G5

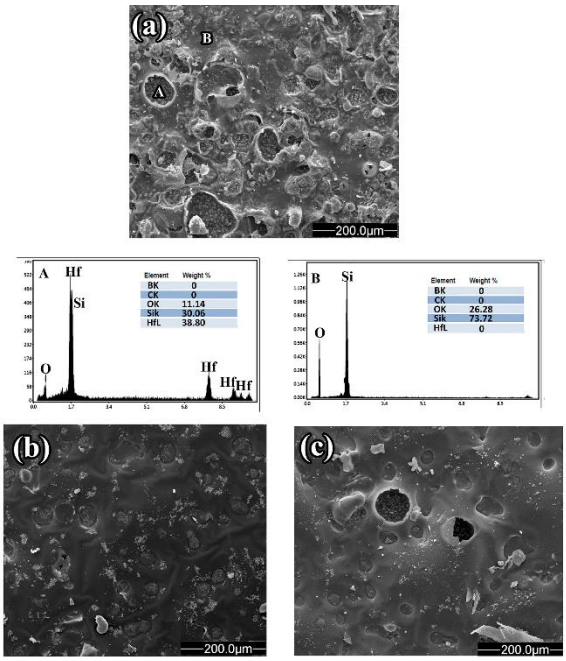

Figure 10. FESEM image and EDS analysis of the surface of the sintered samples after the oxidation test at 1400 °C for 32 h: (a) G0, (b) G2.5 and (c) G5

HSB liquid. In addition, HfO_2 could react with SiO_2 according to reaction (3) and $HfSiO_4$ particles might also be formed. Due to the higher melting points of HfO_2 and $HfSiO_4$ (>2500 °C), as compared to the glass layer (1650°C), the presence and homogeneous distribution of these crystals in the glass layer improved the stability of the glass layer [43]. Also, according to Figure 10, microcracks were observed on the surface of the oxide layer of the sample G0. These cracks could be due to the high porosity of this composite and its higher oxidation rate, leading to the formation of gaseous products (CO_2, CO, SiO, B_2O_3). In addition, as previously mentioned, given the encouragement of the active oxidation of SiC in this composite, due to its high porosity and release of more gaseous SiO, less $HfSiO_4$ was formed on the surfaces of the oxide layer. As a result, the locking effect of $HfSiO_4$ was reduced, ultimately leading to a decrease in the mechanical strength of the oxide layer and cracking of the surfaces. Figure 11 shows the cross-section of the composite samples after the oxidation test. As shown, two layers were formed on the surface of the composites. According to the EDX analysis, the first layer (outer layer) was rich in Si, while the second one had moderate amounts of Si and Hf. The thickness of each layer formed and the weight gain of the HfB_2-based composites after the oxidation test are shown in Figure 12. Comparison of HfB_2-SiC composites containing different amounts of graphite also showed that with increasing the amount of graphite and burning graphite during the oxidation

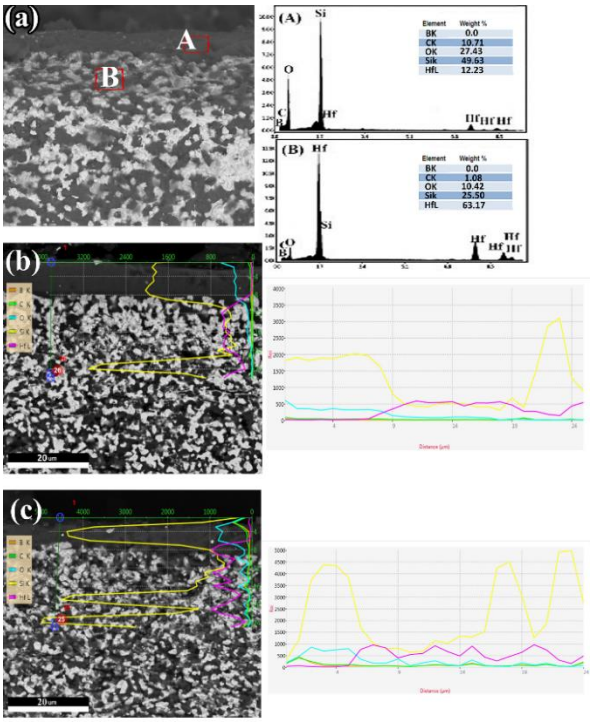

Figure 11. FESEM image of the cross section of the sintered samples after the oxidation test at 1400 °C for 32 h: (a) G0, (b) G2.5 and (c) G5

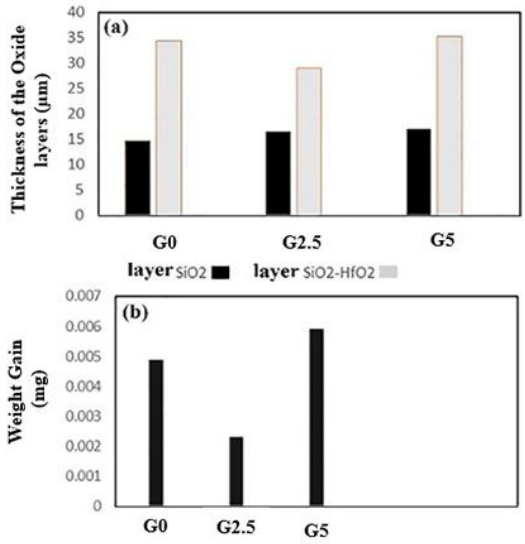

Figure 12. (a) Thickness of oxide layers and (b) weight gain of the sintered samples after the oxidation test at 1400 °C for 32 h

process at 500 °C, along with the formation of new channels for more oxygen to penetrate the composite, the oxidation rate and thickness of the SiO_2 rich layer were increased. However, with increasing the amount of graphite up to 2.5 wt%, due to the formation of a thicker glass layer and the reduced rate of oxygen penetration into the composite, the thickness of the second layer and the increase in the weight of the composite were decreased. Meanwhile, with increasing the amount of graphite up to 5 wt%, due to the lower density of this composite, the thickness of the second layer and weight were raised again. The results of the thermodynamic calculations showed that, due to the high negative free energy in the HfB_2 base composite, reaction (2) occurred at 1400 °C, resulting in HfO_2 and B_2O_3. Oxidation of SiC particles occurred with a lower negative free energy; therefore, SiC particles were then oxidized in two steps. In the first one, the SiC oxidation reaction (1) occurred at the temperature of 1400 °C. On the other hand, the results reported by Mashaykh et al. [46] showed that this reaction could occur at a temperature above 1200 °C. In the second stage of the SiC oxidation process, reaction (6) was performed; as a result, SiO and gaseous CO were formed. Comparing the free energy of reactions (1) and (6) also showed that reaction (1) had occurred; then the SiC particles were oxidized according to the reaction (6). Performing reactions (1) and (6) consistently could lead to the formation of a Si-depleted layer. This layer was not, however, observed in the composites prepared in the present study. It seems, therefore, that the glass phase formed by reaction (1) filled the remaining pores in the composite structure and prevented reaction (6). According to the literature [26, 40], there are three theories to justify the the non-formation of a Si-depleted

layer. According to the first theory, SiO_2 formed during reaction (1) prevented reaction (6) by creating a coating on the composite surface as a diffusion barrier layer. Thus, gaseous SiO and consequently, Si-depleted layer were not formed. The second theory states that even if gaseous SiO is formed during reaction (6), the Si-rich glass layer fills the pores and prevents the gaseous SiO from escaping. Therefore, no Si-depleted layer was observed in the oxidation test. The third theory holds that graphite could increasethe activity of carbon, as compared to sic, thus affecting the CO pressure below the SiO_2 layer. Therefore, the addition of carbon prevented the evaporation of SiC due to drop of the CO pressure and the formation of the Si-depleted layer.

4. CONCLUSION

In the present work, HfB_2-20 SiC composite reinforced with 2.5 and 5% by weight of graphite, as prepared by Spark Plasma Synthesis, and its effects on the microstructure, mechanical properties and oxidation resistance for 32 hours at 1400 ° C were investigated. The addition of graphite improved compressibility due to lubrication and the slip between particles. On the other hand, the hardness of the composite was decreased significantly with the increase of graphite, which could be referred to as inherent softness. Addition of 2.5 %wt graphite increased flexural strength. The HfB_2-20 SiC composite containing 5 %wt graphite had poor oxidation resistance.The reason for encouraging the active oxidation of SiC in this composite was the high porosity and emission of SiO gas, which contained less $HfSiO_4$ at the oxide layer surfaces. As a result, the locking effect of $HfSiO_4$ was reduced, ultimately leading to a reduction in the mechanical strength of the oxide layer and cracking of surfaces.

5. REFERENCES

1. Balak, Z. and Zakeri, M., "Effect of HfB_2 on microstructure and mechanical properties of ZrB_2-SiC-based composites", ***International Journal of Refractory Metals and Hard Materials***, Vol. 54, (2016), 127-137. doi: 10.1016/j.ijrmhm.2015.07.011
2. Shojaie-Bahaabad, M. and Hasani-Arefi, A., "Ablation properties of ZrC-SiC-HfB_2 ceramic with different amount of carbon fiber under an oxyacetylene flame", ***Materials Research Express***, Vol. 7, (2020), doi: 10.1088/2053-1591/ab70db
3. Binner, J., Porter, M., Baker, B., Zou, J. and Venkatachalam, V., "Selection, processing, properties and applications of ultra-high temperature ceramic matrix composites, UHTCMCs – a review", ***International Materials Reviews***, (2019), doi: 10.1080/09506608.2019.1652006
4. Balak, Z. and Azizieh, M., "Oxidation of ZrB_2 -SiC composites at 1600°C : effect of carbides, borides, silicides and chopped carbon fiber", ***Advanced Ceramics Progress***, Vol. 4, (2018), 18-23. doi: 10.30501/ACP.2018.90829
5. Ghadami, S., Taheri-Nassaj, E., Baharvandi, H. R. and Ghadami, F., "Improvement of mechanical properties of HfB_2-based composites by incorporating in situ SiC reinforcement", ***Scientific Reports***, (2021). doi: 10.1038/s41598-021-88566-0
6. Hassan, R., Kundu, R. and Balani, K., "Oxidation behaviour of coarse and fine SiC reinforced ZrB_2 at re-entry and atmospheric oxygen pressures", ***Ceramics International Journal***, Vol. 46, (2020), 11056-11065. doi: 10.1016/j.ceramint.2020.01.125
7. Ghelich, R., Jahannama, M. R., Abdizadeh, H., Torknik, F. S. and Vaezi, M. R., "Hafnium diboride nonwoven mats with porosity/morphology tuned via different heat treatments", ***Materials Chemistry and Physics***, Vol. 248, (2020), doi: 10.1016/j.matchemphys.2020.122876
8. Tian, Y. H., and Dong, L. H., "Effect of mechanical alloying on sinterability and phase evolution in pressure-less sintered TiB_2–TiC ceramics", ***Journal of Materiomics***, Vol. 5, No. 4, (2019), 670-678. doi: 10.1016/j.jmat.2019.05.001
9. Ghadami, S., Taheri-Nassaj, E. and Baharvandi, H. R., "Novel HfB_2-SiC-$MoSi_2$ composites by reactive spark plasma sintering", ***Journal of Alloys and Compounds***, Vol. 809, (2019), doi: 10.1016/j.jallcom.2019.151705
10. Sakkaki, M., Sadegh Moghanlou, F., Vajdi, M. and Shahedi Asl, M., "Numerical simulation of heat transfer during spark plasma sintering of zirconium diboride", ***Ceramics International***, Vol. 46, (2020), 4998-5007. doi: 10.1016/j.ceramint.2019.10.240
11. Liang, X., Wei-Ming, G., Yan, Z., Yang, Y. and Hua-Tay, L., "Pressureless densification of HfB_2-based ceramics using HfB_2 powders by borothermal reduction", ***Ceramics International***, Vol. 47, No. 23, (2021), 33922-33925. doi: 10.1016/j.ceramint.2021.08.245
12. Simonenkoa, E. P., Simonenkoa, N. P. and Lysenkovb, A. S., "Reactive hot pressing of HfB_2–SiC–Ta_4HfC_5 ultra-high temperature ceramics", ***Journal of Inorganic Chemistry***, Vol. 65, No. 3, (2020), 446-457. doi: 10.1134/S0036023620030146
13. EL-Wazery, M. S., "Fabrication and characteristics of 8YSZ/Ni functionally graded materials by applying spark plasma sintering procedure", ***International Journal of Engineering, Transactions C: Aspects***, Vol. 27, No. 12, (2014), 1907-1912. doi: 10.5829/idosi.ije.2014.27.12c.14
14. Mashayekh, S. and Baharvandi, H. R., "Effects of SiC or $MoSi_2$ second phase on the oxide layers structure of HfB_2-based composites", ***Ceramics International Journal***, Vol. 43, (2017), 15053-15059. doi: 10.1016/j.ceramint.2017.08.031
15. Ren, X., Shang, T. and Wang, W., "Dynamic oxidation protective behaviours and mechanisms of HfB_2-20wt%SiC composite coating for carbon materials", ***Journal of the European Ceramic Society***, Vol. 39, (2019), 1955-1964. doi: 10.1016/j.jeurceramsoc.2019.01.033
16. Guerineau, V., Vilmart, G. and Dorval, N., "Comparison of ZrB_2-SiC, HfB_2-SiC and HfB_2-SiC-Y_2O_3 oxidation mechanisms in air using LIF of BO_2 (g)", ***Corrosion Science***, (2019), doi: 10.1016/j.corsci.2019.108278
17. Ghadami, S., Taheri-Nassaj, E., Baharvandi, H. R. and Ghadami, F., "Effect of in situ VSi_2 and SiC phases on the sintering behaviour and the mechanical properties of HfB_2-based composites", ***Scientific Reports***, (2020), doi: 10.1038/s41598-020-73295-7
18. Simonenkoa, E. P., Simonenkoa, N. P., Nagornova, I. A. and Sevastyanova, V. G., "Production and oxidation resistance of HfB_2–30 vol % SiC composite powders modified with $Y_3Al_5O_{12}$", ***Russian Journal of Inorganic Chemistry***, Vol. 65, No. 9, (2020), 1416-1423. doi: 10.1134/S003602362009020X
19. Wang, P., Li, H., Sun, J.,Yuan, R., Zhang, L., Zhang, Y. and Li, T., "The effect of HfB_2 content on the oxidation and thermal shock resistance of SiC coating", ***Surface and Coatings Technology***, Vol. 339, (2018), 124-131. doi:

10.1016/j.surfcoat.2018.02.029

20. Elizaveta, P., Simonenkoa, N. P., Nikolay, P. Simonenkoa, E. P. and Anatoly, F., "Oxidation of HfB_2-SiC-Ta_4HfC_5 ceramic material by a supersonic flow of dissociated air", ***Journal of the European Ceramic Society***, (2020), doi: 10.1016/j.jeurceramsoc.2020.10.001
21. Gurcan, K. and Derin, B., "Effect of SiC particle size on the microstructural, mechanical and oxidation properties of In-situ synthesized HfB_2-SiC composites", ***Politeknik Dergisi***, Vol. 24, No. 2, (2021), 503-551. doi: 10.2339/politeknik.682256
22. Ren, X., Mo, H., Wang, W., Feng, P., Guo, L. T. and Li, Z., "Ultra high temperature ceramic HfB_2-SiC coating by liquid phase sintering method to protect carbon materials from oxidation", ***Materials Chemistry and Physics***, Vol. 217, (2018), 504-512. doi: 10.1016/j.matchemphys.2018.07.018
23. Guo, S., "Oxidation and strength retention of HfB_2−SiC composite with La_2O_3 additives", ***Advances in Applied Ceramics***, (2020), doi: 10.1080/17436753.2020.1755510
24. Opila, E., Levine, S., and Lorincz, J., "Oxidation of ZrB_2- And HfB_2-based ultra-high temperature ceramics: Effect of Ta additions", ***Journal of Materials Science***, Vol. 39, (2004), 5969-5977. doi: 10.1023/B:JMSC.0000041693.32531.d1
25. Rezaie, A., Fanrenholtz, W. G. and Hilmas, G. E., "Oxidation of zirconium diboride-silicon carbide at 1500°C at a low partial pressure of oxygen", ***Journal of the American Ceramic Society***, Vol. 89, (2006), 3240-3245. doi: 10.1111/j.1551-2916.2006.01229.x
26. Rezaie, A., Fahrenholtz, W. G. and Hilmas, G. E., "The effect of a graphite addition on oxidation of ZrB_2-SiC in air at 1500°C", ***Journal of the European Ceramic Society***, Vol. 33, (2013), 413. doi: 10.1016/j.jeurceramsoc.2012.09.016
27. Zamora, V., Nygren, M., Guiberteau, F. and Ortiz, A. L., "Effect of graphite addition on the spark-plasma sinterability of ZrB_2 and ZrB_2–SiC ultra-high-temperature ceramics", ***Ceramics International***, Vol. 40, (2014), 11457-11464. doi: 10.1016/j.ceramint.2014.03.130
28. Shahedi Asl , M., Zamharir, M. J., Ahmadi, Z. and Parvizi, S., "Effects of nano-graphite content on the characteristics of spark plasma sintered ZrB_2–SiC composites", ***Materials Science and Engineering A***, Vol. 716, (2018), 99-106. doi: 10.1016/j.msea.2018.01.038
29. Azizian-Kalandaragh, Y., Namini, A. S., Ahmadi, Z. and Shahedi Asl, M., "Reinforcing effects of SiC whiskers and carbon nanoparticles in spark plasma sintered ZrB_2 matrix composites", ***Ceramics Internationa,*** Vol. 44, (2018), 19932-19938. doi: 10.1016/j.ceramint.2018.07.258
30. Nasiri, Z. and Mashhadi , M., "Microstructure and mechanical behavior of ternary phase ZrB_2-SiC-AlN nanocomposite", ***International Journal of Refractory Metals and Hard Materials***, Vol. 78, (2019), 186-192. doi: 10.1016/j.ijrmhm.2018.09.009
31. Sergey, N., "Processing and characterization of spark plasma sintered SiC-TiB_2-TiC powders", ***Materials***, Vol. 15, No. 5, (2022), 1946. doi: 10.3390/ma15051946
32. Shahriari, M., Zakeri. M., Razavi, M. and Rahimipour, M. R., "Investigation on microstructure and mechanical properties of HfB_2.SiC-HfC ternary system with different HfC content prepared by spark plasma sintering", ***International Journal of Refractory Metals and Hard Materials***, Vol. 93, (2020), 105350. doi: 10.1016/j.ijrmhm.2020.105350
33. Emami, S. M., Salahi, E., Zakeri, M. and Tayebifard, S. A., "Effect of composition on spark plasma sintering of ZrB_2–SiC–ZrC nanocomposite synthesized by MASPSyn", ***Ceramics International***, Vol. 43, (2017), 111-115. dot: 10.1016/j.ceramint.2016.09.118
34. Shahedi Asl, M., "Microstructure, hardness and fracture toughness of spark plasma sintered ZrB_2–SiC–Cf composites", ***Ceramics International***, Vol. 43, (2017), 15047-15052. doi: 10.1016/j.ceramint.2017.08.030
35. Shahedi Asl, M., Pazhouhanfar, Y., Sabahi Namini, A., Shaddel , S., Fattahi, M. and Mohammadi, M., "Role of graphite nano-flakes on the characteristics of ZrB_2-based composites reinforced with SiC whiskers", ***Diamond and Related Materials***, Vol. 105, (2020), 107786. doi: 10.1016/j.diamond.2020.107786
36. Yuan, Y., Liu, J. X. and Zhang, G. J., "Effect of HfC and SiC on microstructure and mechanical properties of HfB_2-based ceramics", ***Ceramics International***, Vol.42, (2016), 7861-7867. doi: 10.1016/j.ceramint.2016.01.067
37. Hosseinia, Z., Mollazadeh Beidokhti, S., Vahdati Khakib, J. and Pourabdoli, M., "Preparation of porous alumina/nano-nickel composite by gel casting and carbothermic reduction", ***International Journal of Engineering, Transaction A: Basics***, Vol. 35, No. 01, (2022), 220-227. doi: 10.5829/IJE.2022.35.01A.21
38. Sabree, I. K., Aswad, M. A. and Abd Ali, H. S., "Effect of additional zirconia on fracture mechanics of bioactive glass-ceramics using digital image correlation", ***International Journal of Engineering, Transactions C: Aspects***, Vol. 34, No. 9, (2021), 2053-2059. doi: 10.5829/IJE.2021.34.09C.02
39. Taghian Dehaghani, M. and Ahmadian, M., "Fracture mechanism of CoCrMo porous nano-composite prepared by powder metallurgy route", ***International Journal of Engineering, Transaction A: Basics***, Vol. 31, No. 1, (2018), 19-24. doi: 10.5829/ije.2018.31.01a.03
40. Ghadami, S., Taheri-nassaj, E., Baharvandi, H. R. and Ghadami, F., "Effect of in situ SiC and $MoSi_2$ phases on the oxidation behavior of HfB_2 - based composites", ***Ceramics International Journal***, Vol. 46, (2020), 20299-20305. doi: 10.1016/j.ceramint.2020.05.116
41. Wang, P., Li, H., Sun, J., Yuan, R., Zhang, L., Zhang, Y. and Li, T., "The effect of HfB_2 content on the oxidation and thermal shock resistance of SiC coating", ***Surface & Coatings Technology***, Vol. 339, (2018), 124-131. doi: 10.1016/j.surfcoat.2018.02.029
42. Jin, H., Meng, S., Zhang, X., Zeng, Q. and Niu, J., "Effects of oxidation temperature, time and ambient pressure on the oxidation of ZrB_2 – SiC-graphite composites in atomic oxygen", ***Journal of the European Ceramic Society***, Vol. 36, (2016), 1855-1861. doi: 10.1016/j.jeurceramsoc.2016.02.040
43. Ren, X., Mo, H., Wang, W., Feng, P., Guo, L. and Li, Z., "Ultra high temperature ceramic HfB_2-SiC coating by liquid phase sintering method to protect carbon materials from oxidation", ***Materials Chemistry and Physics***, (2018), doi: 10.1016/j.matchemphys.2018.07.018

Persian Abstra

چکیده

در مطالعه حاضر، کامپوزیت‌های HfB_2-SiC-graphite به روش سنترینگ پلاسمای جرقه‌ای در دمای ℃ ۱۹۰۰ به مدت ۱۰ دقیقه تهیه شدند. تاثیر مقدار گرافیت بر ریزساختار، خواص مکانیکی مطالعه شد. همچنین مقاومت به اکسیداسیون کامپوزیت‌های اماده شده در دمای ℃ ۱٤۰۰ به مدت ۳۲ ساعت بررسی شد. تغییرات وزن و ضخامت لایه اکسیدی تشکیل شده بر روی سطح کامپوزیت اندازه‌گیری شد. دانسیته نسبی، چقرمگی و استحام کامپوزیت‌های سینتر شده با افزایش مقدار گرافیت تا ۲/۵ درصد وزنی افزایش یافت و سپس کاهش یافت. سختی کامپوزیت‌ها وقتی گرافیت افزوده شد، کاهش یافت. مقاومت به اکسیداسیون کامپوزیت بعد از افزودن گرافیت تا ۲/۵ درصد وزنی بهبود یافت در حالیکه مقدار اضافی گرافیت سبب افت مقاومت به اکسیداسیون کامپوزیت شد.